Title	Sustained smooth dynamics in short-sleeved nanobearings based on double-walled carbon nanotubes
Author(s)	Shenai, Prathamesh Mahesh; Ye, Jun; Zhao, Yang
Citation	Shenai, P. M., Ye, J. & Zhao, Y. (2010). Sustained smooth dynamics in short-sleeved nanobearings based on double-walled carbon nanotubes. Nanotechnology, 21.
Date	2010
URL	http://hdl.handle.net/10220/6919
Rights	© 2010 Institute of Physics. This is the author created version of a work that has been peer reviewed and accepted for publication by Nanotechnology, Institute of Physics. It incorporates referee's comments but changes resulting from the publishing process, such as copyediting, structural formatting, may not be reflected in this document. The published version is available at: [http://dx.doi.org/10.1088/0957-4484/21/49/495303].

Sustained smooth dynamics in short-sleeved nanobearings based on double-walled carbon nanotubes

Prathamesh M Shenai, Jun Ye and Yang Zhao*

School of Materials Science and Engineering, Nanyang Technological University, 639789, Singapore

*E-mail: YZhao@ntu.edu.sg

Abstract

We carry out a molecular dynamics study of nanobearings based on double-walled carbon nanotubes with a short rotating outer tube. A (4, 4)/(9, 9) bearing configuration shows peculiar stabilization of rotational motion at certain values of angular velocities. The observed trend is found at those values of initial angular velocities (in the current context, 0.8–1.5 rad ps^{-1}) which denote a transitional regime between nearly frictionless operation at low initial angular speeds and decaying performance at high initial angular velocities. With the use of detailed 'principal components analysis', we find that the energy dissipation occurs mainly due to the excitation of wavy modes in the inner tube of the bearing. It is also proposed that wavy deformation is facilitated by the actuation of axial translation of the outer tube, which acts as an energy channelling mode. Hence, we find that the absence of dissipative wavy modes results in sustained smooth rotational dynamics of the nanobearing at low temperature.

Online supplementary data available from stacks.iop.org/Nano/21/495303/mmedia

---

1. Introduction

'Carbon nanotubes' (CNTs) have become ubiquitous keywords across all areas of nanotechnology. The unique structure of a single-walled carbon nanotube (SWNT) consists of a cylindrically wrapped sheet of carbon atoms networked via sp^2 hybridized bonds [1]. Bestowed with exceptionally high mechanical strength and interesting electronic properties, CNTs have garnered a tremendous amount of research momentum. Multi-walled carbon nanotubes (MWNTs) are extremely interesting structures. MWNTs consist of concentric SWNTs, which are structurally strong elements separated from each other by an equilibrium inter-tube distance of 0.34 nm as dictated by the weak van der Waals interactions. Hence, such a structure is ideally suited for actuating relative inter-tube sliding and rotation with shallow frictional resistance. Sophisticated and promising

technologies for the manipulation of individual CNTs have raised the possibilities of the construction of simple devices such as an oscillator or a rotational bearing [2–5]. Although the technological front is well paced, it faces extreme challenges. On the other hand, theoretical performance studies of nanodevices constructed from double-walled carbon nanotubes (DWNTs) have been undertaken in detail in the last decade. Apart from the most simple operation of a device such as an oscillator or a rotational bearing, many other devices such as cap springs [6], surface profiling devices [7], molecular pumps [8, 9], motor engines [10] and mass sensors have been conceptually presented. Such studies are inevitable to precede the actual implementation of molecular devices.

Many theoretical and molecular dynamics studies have established that a simple DWNT oscillator can operate at gigahertz or even higher frequency regimes [11–13]. Their rotational counterparts, bearings produced using DWNTs, also follow the same course [18]. Ideal conditions prescribe that the atomically smooth contact surfaces should offer negligibly small frictional resistance to any inter-tube relative motion in DWNT-based machines. However, a variety of factors such as contact area, tube commensuration, excitation of non-rigid body dissipative modes, and operating velocities and temperatures affect the function of a nanomachine, eventually leading to a possible failure. Many different quantifications of the energy dissipation have been proposed [13–17]. In essence, friction in the nanomachines is characterized by excitation of high frequency phonon modes that are reflected in terms of a temperature increase.

Rotational nanobearings have been shown to exhibit a characteristic threshold velocity of operation [18–20]. Zhang *et al* found that rapid failure of a bearing may occur if spun at higher than a threshold velocity [18]. DWNT bearing configurations with the equilibrium inter-tube distance of 0.34 nm exhibit smoother rotation while deviation from the equilibrium distance leads to reduced operation. Servantie and Gaspard have proposed a linear dependence of dynamical frictional dissipation on the contact area in a DWNT rotational bearing, which is corroborated by a few molecular dynamics studies [16]. At the same time, the frictional characteristics in such devices can be sensitive to the geometry as well. Excitation of wavy deformation modes was attributed to the primary mechanism of energy dissipation in nano-oscillators with long inner tubes [13]. On the other hand, when the oscillating inner tube is comparatively short, off-axial rocking modes prevail to cause energy decay. While downplaying the role of overlap area in causing friction in the case of very long oscillators, Tangney *et al* argued for the significance of the interactions due to tube edges [17]. Efforts have also been made to examine the effects of defects [21–23] or the temperature dependence of nanodevice operation, leading to contentious results. Among all, however, unanimity seems to prevail in the view of the critical importance of operational velocity in both the oscillators and the bearings. In oscillators, at very slow sliding speeds, the friction is expected to show a linear increase with velocity [15]. At high velocities, a nonlinear

dependence is speculated to appear in the picture [17]. A couple of studies indicate, in an otherwise smooth oscillator, a very strong enhancement of friction at some peculiar sliding speeds [15, 24, 25]. Resonant excitations of modes such as various radial breathing modes was found responsible in giving rise to this phenomenon.

In this paper, we study a specific configuration of a DWNT-based nanobearing in which a short outer tube acts as a rotating sleeve. Due to the small length of the sleeve, the operation of this bearing is peculiarly different from a similar bearing but with both tubes of equal length. We find the tendency of such a bearing to sustain a nearly frictionless operation at low initial angular velocities or to undergo significant dissipation at high initial angular velocities. In the intermediate range of angular velocities (e.g. 0.8–1.5 rad ps^{-1} for a short-sleeved configuration of (4, 4)/(9, 9) DWNT), we find that the decay in the rotational speeds is characterized by different plateaus. The observed behaviour bears some resemblance to the previous reports concerning DWNT oscillators. We examine the bearing performance and assess the factors that introduce a decay in its rotational speed.

The rest of this paper is organized as follows. Section 2 introduces the details of the DWNT bearing structure and molecular dynamics simulations employed. Section 3 consists of the results of the bearing simulations. Peculiarities observed in the bearing operation are probed in detail and the investigation of the underlying causes is discussed. Conclusions are drawn in the final section 4.

2. Molecular dynamics simulations

The rotational nanobearings in this paper are constructed from a DWNT structure with a (4, 4) nanotube as the inner tube and a (9, 9) nanotube as the outer tube. The length of the inner tube is 9.70 nm while the outer tube length is varied in different configurations. In the optimized structures of (4, 4)/(9, 9) DWNTs, both tubes share a common centre of mass as shown in figure 1. In all our molecular dynamics simulations, the outer sleeve serves as a rotator of the bearing and the inner tube acts as a shaft. Rotational motion is generated by ascribing an initial angular velocity to every atom of the sleeve prior to the simulation. Three atoms at each end of the shaft were frozen at their initial positions. In order to examine the influence of topological defects, a similar bearing structure with a single vacancy defect introduced at the mid-length of the sleeve is utilized. As described later, due to its intriguing rotational characteristics, the current work mostly focuses on the operation of a (4, 4)/(9, 9) DWNT configuration with 1.84 nm long sleeve containing a single vacancy defect at its mid-length. Geometry optimization and dynamics calculations are performed using the Dreiding force field [26], which has been utilized in some previous molecular dynamics studies on CNTs [27, 28]. Geometry optimization is carried out with steepest-descent, conjugate-gradient and

Newton-minimizer algorithms, each applied at a different stage during the optimization process. All the simulations are performed in a microcanonical ($NV\,E$) ensemble and without any pre-simulation heating. Inter-tube interactions are modelled by the Lennard-Jones (L-J 12-6) potential which has the form: $V(R) = D_0[(R_0/R)^{12} - 2(R_0/R)^6]$. The L-J 12-6 potential is parametrized with the values ($D_0 = 0.0951$ kcal mol^{-1} and $R_0 = 3.89$ Å) taken from the Dreiding force field [26]. Molecular dynamics calculations make use of a Verlet velocity integration scheme with a time step of 1 fs. This typical time step value is small enough to avoid the discretization errors while being sufficient enough to produce production simulation runs of the order of nanoseconds. Various other DWNT configurations (3, 3)/(8, 8); (5, 5)/(10, 10); (6, 6)/(11, 11); (7, 0)/(9, 9); (5, 0)/(14, 0) and (6, 6)/(19, 0) in a short-sleeved geometry (shaft and sleeve lengths nearly 10 nm and 2 nm, respectively) are also examined.

3. Results and discussions

Performance of a DWNT nanobearing may depend significantly on the area of contact [16, 17]. To probe this situation, we utilize different (4, 4)/(9, 9) bearing configurations with sleeve lengths varying from 1.84 to 9.7 nm, subjected to a certain initial angular velocity (ω_0). Figure 2 shows the rotational velocity of the sleeve in all these bearings at $\omega_0 = 1$ rad ps^{-1}. It is evident that, for the configurations with sleeves longer than 2.82 nm, the rotation takes place in a wearless manner. However, the bearing with a sleeve of length 1.84 or 2.82 nm, shows strikingly different features. Specifically for the bearing with 1.84 nm long sleeve, two distinct regimes, a dissipative one and one with stable rotation, can be observed. During the first 200 ps, the angular velocity shows a steady decrease followed by a sharper dip. However, after this initial period of dissipation, the rate of decrease in the angular velocity is imperceptibly slow, implying a very smooth and near-frictionless rotation. It is clear that such an intriguing character of dissipation of rotational kinetic energy, followed by its smooth stabilization, is specific to only those configurations with short sleeves. Size dependence may also point towards possible edge effects. As the sleeve length is reduced, the interactions between the atoms of the shaft and at the ends of the sleeve become more significant. Since the edge atoms are accompanied by dangling bonds, with the smaller size of the sleeve, their contribution to the overall interactions may become higher. It is interesting to note the initial reduction in the angular velocity and its subsequent levelling off. For an infinitely long inner tube, simulated using periodic boundary conditions and without any atoms fixed in position, this trend vanishes completely and angular velocity is preserved well at its initial value.

Earlier studies indicate that, under suitable conditions, the presence of even a single vacancy or Stone–Wales defect may introduce significant impacts on the performance of DWNT nanodevices. Due to the small size of the sleeve in our bearing configuration, it is possible that a small density of defects may disturb the angular velocity flattening behaviour. Bearing

simulations were then performed on a similar (4, 4)/(9, 9) DWNT bearing but with a single vacancy defect introduced at the middle of the outer tube. The essential characteristics of the angular velocity dissipation were found to be preserved even in the presence of single vacancy defects. Further, since in comparison to the perfect structure the bearing with a vacancy defect showed slightly better stabilization of angular velocity, we use the latter configuration for extensive analysis hereafter.

The same initial structure of the (4, 4)/(9, 9) bearing with a single vacancy is then subjected to a wide range of initial angular velocities ranging from 0.7 to 2 rad ps^{-1}. Figure 3 exhibits the angular velocity dampening with time for all these configurations. It can be readily observed that the distinctive behaviour of dissipation and flattening occurs only in a range of initial angular velocities. At and below 0.7 rad ps^{-1} of initial angular velocity, there is no loss of rotational kinetic energy, and the rotation is maintained smoothly around the original value. On the other hand, when the initial angular speed exceeds 1.5 rad ps^{-1}, the bearing enters into a dissipative mode in which the angular velocity gets decayed continuously. For the cases with angular velocities ranging between these two extremes, the peculiarity of the dissipative trend is evident. The observed behaviour can then be said to lie on the boundary of a transition from a nearly wearless rotation to a dissipative regime. It is further interesting to observe that, for most of the cases, there occur multiple velocity plateaus. With initial angular velocity 1.2 rad ps^{-1}, the first 300 ps show smooth rotation, followed by dampening of rotation for the next 100 ps. Another period of placid rotation occurs for the next 400 ps during which the angular velocity is maintained roughly at 1.05 rad ps^{-1}. Then, it again enters a dissipative mode until about 1250 ps when another plateau appears at the velocity of 0.7 rad ps^{-1}. A close observation of all the peculiar cases reveals certain even finer angular velocity ranges in which this particular configuration of a (4, 4)/(9, 9) bearing with vacancy rotates in a frictionless manner. Such possibly stable ranges of angular velocities are highlighted in figure 3. A bearing which is rotating close to such a stable range attempts to stabilize itself by moving in this region. When the stabilization is not successful, or becomes ephemeral, its angular velocity continues to reduce until the next lower stable range is encountered. A dramatic increase in frictional effects is reported previously in DWNT configurations when the inner tube is sliding at certain critical speeds [24, 25]. The interesting analogy of our findings for the rotational bearings will be discussed later.

As the molecular dynamics simulation is performed without any pre-simulation heating, the atoms of both the tubes gain disorderly kinetic energies as soon as the simulation commences. Relative kinetic energy (K_{rel}) serves as a direct measure of the disorderly phonon energy [13]. The frame of reference is chosen such that the axis of both the tubes, which passes through their centre of mass, is aligned along the z axis. After adapting the approach of Zhao *et al* [13] to take into account the rotational motion, the expression for K_{rel} can be formulated as

$$K_{\text{rel}} = \sum_i \tfrac{1}{2} m_i |\vec{v}_i^{\text{inn}} - \vec{v}_{\text{ave}}^{\text{inn}} - \vec{\omega}_{\text{ave}}^{\text{inn}} \times \vec{r}_i^{\text{inn}}|^2 + \sum_j \tfrac{1}{2} m_j |\vec{v}_j^{\text{out}} - \vec{v}_{\text{ave}}^{\text{out}} - \vec{\omega}_{\text{ave}}^{\text{out}} \times \vec{r}_j^{\text{out}}|^2 \quad (1)$$

where m_i (m_j) and $\vec{v}_i^{\text{inn}}$ ($\vec{v}_j^{\text{out}}$) are the mass and the velocity of the i th (j th) atom of the inner (outer) tube, respectively, and $\vec{v}_{\text{ave}}^{\text{inn}}$ ($\vec{v}_{\text{ave}}^{\text{out}}$) denotes the average velocity of the inner (outer) tube. The average angular velocity of the inner (outer) tube is represented by $\vec{\omega}_{\text{ave}}^{\text{inn}}$ ($\vec{\omega}_{\text{ave}}^{\text{out}}$) and $\vec{r}_i^{\text{inn}}$ ($\vec{r}_j^{\text{out}}$) denotes the radial position of the i th (j th) atom of the inner (outer) tube from the z axis.

Treating the instantaneous structure of a DWNT bearing as a rigid body if the off-axial deviations and tube deformations are not significantly high, an alternative formula for relative kinetic energy (E_{rel}) can also be proposed solely in terms of different kinetic energies:

$$E_{\text{rel}} = \left(\sum_i \tfrac{1}{2} m_i |\vec{v}_i^{\text{inn}}|^2 + \sum_j \tfrac{1}{2} m_j |\vec{v}_j^{\text{out}}|^2 \right) - \left[\sum_i \tfrac{1}{2} m_i (v_{\text{ave-z}}^{\text{inn}^2} + d_i^{\text{inn}^2} \omega^{\text{inn}^2}) + \sum_j \tfrac{1}{2} m_j (v_{\text{ave-z}}^{\text{out}^2} + d_j^{\text{out}^2} \omega^{\text{out}^2}) \right] \quad (2)$$

where $v_{\text{ave-z}}^{\text{inn}}$ ($v_{\text{ave-z}}^{\text{out}}$) is the speed of the centre of mass of the inner (outer) tube along the z axis and ω^{inn} (ω^{out}) is the average angular speed of the inner (outer) tube about the z axis. d_i^{inn} $\left(d_j^{\text{out}}\right)$ is the radial distance of the i th (j th) atom of the inner (outer) tube from the z axis, respectively. In equation (2), the sum of the terms in the first bracket gives the total kinetic energy of the system while that in the square bracket represents the group translational and rotational kinetic energy components for the shaft and the sleeve. For the purpose of this paper, we utilize equation (2) for the calculation of E_{rel}.

As all the initial kinetic energy of the system prior to the start of the simulation is composed of the rotational kinetic energy of the sleeve, we may associate no pre-simulation temperature with the system. Relative kinetic energy can then be used as a measure of rising system temperature as $T = 2E_{\text{rel}}/((3N - 6)k_{\text{B}})$, where N is the total number of atoms and k_{B} is the Boltzmann constant. In our simulations, we observe a maximum increase of temperature due to heating caused by frictional dissipation to be about 27 K (when ω_0 = 1.1 rad ps^{-1}). This reflects the extremely low temperature at

which the bearing operates. At higher operating temperatures such as at room temperature, the temperature effects may lead to less dramatic characteristics of angular velocity behaviour. Friction in the nanoscale devices is usually evaluated as the acquisition of the disorderly phonon energies. Therefore at an elevated temperature, thermal effects are expected to enhance the friction in the system affecting the energy dissipation characteristics. We have also studied the operation of the (4, 4)/(9, 9) bearing with a vacancy defect on the sleeve when it is heated to 298 K (by using *NVT* simulation) prior to the *NVE* simulation (see the supplementary material available at stacks.iop.org/Nano/21/495303/mmedia). At higher temperature, the tendency of the bearing towards angular velocity stabilizations is subdued. The bearing undergoes steady overall dissipation until it stabilizes only at a lower angular velocity. The intermediate angular velocity plateaus do not occur. Stabilized rotation is also accompanied by a small rate of energy dissipation in contrast to a near-perfect stabilization for the bearing with no pre-simulation heating. Nevertheless, the signature of relaxation of the bearing to a stable operational angular velocity is detectable during its operation at a high temperature.

Apart from the excitation of high frequency disorderly modes, other mechanical modes are also actuated, the most prominent of which is the translation of the sleeve. Figure 4(b) shows the axial displacement of the sleeve during the simulation when initiated at ω_0 = 1 rad ps^{-1}. A clear correlation between the angular velocity dampening and the large scale axial motion can also be observed. During the first 150 ps, the sleeve gains sufficient translational kinetic energy so as to undergo a continuous, large amplitude axial motion. Beyond that, the translational motion ceases and the sleeve keeps oscillating within a very narrow potential well along the axial direction. The shift in the trend of translational motion coincides with that for its rotational motion. Sliding of the sleeve for the case of $\omega_0 =$ 0.7 rad ps^{-1} is, however, observed to be restricted to a narrow axial range. For this stable configuration, the sleeve does not gain enough energy to overcome the axial energy barrier between the adjacent energy grooves. On the other hand, in the case of $\omega_0 = 2$ rad ps^{-1}, the sleeve undergoes a continuous and large amplitude motion along the axis, which is also reflected in the continuously decaying angular velocity.

Owing to its small size, the very small inertia of the sleeve makes it easier to set itself into translational motion by channelling the energy from the rotational kinetic energy. However, its small mass also implies that, although the motion is long ranged, the translational kinetic energy acquired is quite small. For the bearing at $\omega_0 = 1.0$ rad ps^{-1}, figure 4(c) displays that the translational kinetic energy of the sleeve is negligibly low from 200 ps onwards when compared to the loss of rotational kinetic energy. Even during the first 200 ps, when it sweeps along the axis, its translational kinetic energy is at least an order of magnitude lower than the loss in the rotational kinetic energy. On the other hand, the relative kinetic energy increases significantly, indicating the thermal energy acquisition in the system. The axial actuation of

the sleeve is thus not sufficient alone to explain the dampening behaviour. It is still possible that various other phonon modes may get excited due to the linear motion of the sleeve. In such a case, the translational motion of the sleeve may serve as merely a channel to withdraw energy from the rotational mode and excite the dissipative phonon modes. When the linear movement of the sleeve nearly comes to a halt, this channel gets blocked and no further phonon modes can be excited.

While the axial motion of the outer tube appears significant in the foregoing discussion, the contribution from the modes excited in the inner tube is equally important. The actual energy loss from the rotational mode gets reflected in the disorderly phonon modes excited in both tubes. In order to probe the excitation and the relevance of various modes of vibration, we use a standard statistical technique—principal components analysis (PCA). As an extensively used technique in the study of biomolecules such as proteins, it is applied to reveal the internal motions of the molecule and isolate distinctive modes [29, 30]. With the time-dependent atomic positions for the whole trajectory, a covariance matrix is first constructed with the elements

$$C_{ij} = \langle (x_i - \langle x_i \rangle)(x_j - \langle x_j \rangle) \rangle \tag{3}$$

where x_i is the ith coordinate variable (x, y or z coordinate), The averaging is carried over the complete trajectory time.

After the diagonalization of the covariance matrix, eigenvalues are obtained which denote the relative contributions of the corresponding eigenmodes towards the dynamical motion of the system. Such modes include rigid body mechanical modes such as translation and rotation as well as various other non-rigid body phonon modes. A molecular dynamics package, GROMACS 4.3, is used to carry out PCA on the atomic trajectories over various time periods or over the entire simulation time [31]. Figure 5 shows the eigenvalue plot against indices of the first 50 principal eigenmodes (also called a scree plot), during the simulation time of 1 ns, for three cases ($\omega_0 = 0.7$, 1 and 1.2 rad ps^{-1}). The first three principal modes in this scree plot with the highest eigenvalues contributing to most of the dynamics of the system and standing for the mechanical modes such as rigid body translation and rotation. Modes with higher indices have eigenvalues at least an order of magnitude smaller and are the high frequency vibrational modes such as wavy modes, rocking modes or modes similar to radial breathing. As compared to the bearing initiated at $\omega_0 = 0.7$ rad ps^{-1}, the other two systems show pronounced excitation of modes with higher indices and with eigenvalues larger by at least an order of magnitude. This clearly signifies the lack of excitation of disorderly phonon modes for the bearing running at the lowest angular speed.

Projections of individual eigenvectors on the original trajectory may be utilized to reveal the time-dependent contributions of the identified excited modes. Projections (P) of individual eigenvectors on the original trajectory (represented by a zero mean matrix X such that $X_{t,i} = x_i - \langle x_i \rangle$) can be obtained as $P = XT$, where T is the matrix of column eigenvectors. The original trajectory can be reconstructed easily as PT^{T}. It is of further interest to generate a filtered trajectory (F) by multiplying identically selected subsets from both P and T^{T}, which then contain the motions only along these specific eigenvectors. A filtered trajectory can be obtained in this way helping identify the corresponding mode. Similar analysis carried out in different time periods covering the simulation time may then be expected to reveal progressive excitations of different modes in the system.

We analysed the trajectory data during 0–500 ps for a bearing initiated at $\omega_0 = 1.2$ rad ps^{-1}, which shows the first dissipative period during 270–400 ps. We examined in detail the first eight eigenvectors during every 100 ps from the start of the simulation to 500 ps, their projections on the original trajectory and the corresponding filtered trajectories. Along the same line, the total trajectory from 0 to 500 ps is also analysed. All the corresponding scree plots qualitatively possess the same attributes of having the first three index modes at relatively high eigenvalues. One of the three modes can be identified as the translational mode while the inter-tube rotational mode is represented by the other two modes, in combination. Hence, these first three modes together represent the net translation and rotation of the outer tube. Projections of the first four eigenvectors for the total trajectory during 0– 500 ps are shown in figure 6. The modes with higher indices in different periods are various wavy, off-axial and bending modes. In particular, the fourth indexed mode excited during 300–400 ps is identified as one of the prominent wavy modes and is illustrated in figure 6(e). We observe from the 100 ps split trajectories that it stays absent in the first few modes during the initial 200 ps of non-dissipative rotation of the bearing. It marks the appearance during 200–300 ps of a lower indexed (fifth) mode before gaining significance at the fourth index during 300–400 ps. Its subsequent disappearance occurs after 500 ps and coincides with the onset of stable rotation. In other words, this particular wavy mode of the inner tube lies at a higher index before it gains significance and acts as the energy drain during 300–400 ps. Over the complete trajectory of 0–500 ps, it is identified as the fourth indexed mode as shown in figure 6(d). Clearly, its contribution can be seen to increase at around 270 ps and starts to recede at about 500 ps. It is thus identified as the prominent mode into which the rotational kinetic energy of the bearing gets dissipated.

It is also interesting to analyse the projections of those modes which denote the axial motion of the sleeve. From the PCA on each of the independent trajectory segments, the eigenvector which represents the translational motion is identified and its projection on the original trajectory is plotted in figure 7. As the translational eigenvector comprises a

contribution from the z coordinate of the sleeve, its projection on the trajectory highlights the features of the axial motion.

The projection curves have step-like features for all the trajectories except during 300–400 ps. This indicates that the axial sliding of the sleeve is composed of small steps along the length of the inner tube. In the initial 200 ps (figures 7(a) and (b)), the displacement of the sleeve along the axis is small. The operation of the bearing is quite stable in this period and the relative kinetic energy also remains negligible. During 200–300 ps, the sleeve starts to gain more translational kinetic energy and is displaced to a larger extent, also in a step-like manner (figure 7(c)). The stepwise characteristic is indicative that the translation of the sleeve takes place at an energy sufficient to overcome the subsequent axial potential energy barriers. This picture can be further assisted with the interaction potential energy profile of the system when the sleeve is moved rigidly along the common axis, as shown in figure 8. Although the energy surface resulting from static calculations gets easily perturbed as the simulation progresses, it is very helpful in a qualitative assessment. In the case of the bearing initiated at $\omega_0 = 1.2$ rad ps^{-1}, during the first 200 ps, the maximum translational kinetic energy the sleeve possesses is found to be 11.3 μeV/atom. This value is comparable to the height of subsequent potential energy hills of nearly 10 μeV/atom as the sleeve moves along the axis (see inset, figure 8)

However, during 300–400 ps (figure 7(d)), this character of the sliding breaks down and a smooth sliding motion ensues. During this period, the sleeve thus carries translational kinetic energy in excess to that needed for the stepped axial motion. It is possible that such an energy excess gets expended in exciting modes such as the wavy or bending modes. From figure 6(d), it is well correlated by the strong excitation of the wavy mode(the fourth indexed principal mode) appearing at about 280 ps. Subsequently, after about 400 ps, the sleeve loses most of its translational kinetic energy, indicating the transfer to the dissipative wavy modes. Evident from figures 7(e) and (f), between 400 and 600 ps, the characteristic step-like motion of the sleeve along the axis is restored. Further, the same argument also holds when comparing the bearings showing little dissipation throughout (e.g. at $\omega_0 = 0.7$ rad ps^{-1}) to the dissipation-prone bearing runs. For the bearing with $\omega_0 = 0.7$ rad ps^{-1}, the sleeve movement is observed to be restricted between the adjacent potential energy hills along the common axis throughout the entire simulation period. Such a stark contrast further supports our contention that the axial translational mode may then be considered acting as a channel to divert energy to the dissipative modes.

Servantie and Gaspard first reported signatures of resonance phenomena that lead to enhanced damping of oscillation amplitude in armchair–armchair DWNT oscillators, at certain sliding velocities [15]. A power law dependence of the critical speeds on the radius of the outer tube suggested possible occurrences of radial breathing modes. A few following studies on DWNT configurations with the inner tube sliding inside the outer tube also reported

abrupt enhancement in frictional effects at certain critical sliding speeds [24, 25]. For a (7, 7)/(12, 12) DWNT configuration, Xu *et al* reported that, if the inner tube is sliding at a velocity that falls in a critical speed range, frictional effects increase by many times and, after losing the translational kinetic energy, it may sustain axial sliding at a lower stabilized velocity [24]. Except at the critical axial speeds, the sliding of the inner tube occurs smoothly. The abrupt energy dissipation was attributed to resonant excitation of phonons whose group velocity is similar to the axial inter-tube velocity. Contribution from radial-breathing-like modes excited resonantly by internal mode coupling was shown as significant towards explaining the energy dissipation mechanisms. Our observations in the case of the short-sleeved rotational nanobearings are somewhat similar, yet bear interesting differences. The nanobearings are characterized by a tendency to rotate smoothly at certain angular velocities. However, the smooth rotational motion may get hampered by the excitation of dissipative modes like wavy modes in the inner tube. The wavy modes, in turn, get excited by the actuation of the translational motion of the sleeve. As a result of the energy dissipation, the angular speed of the bearing is depleted to the next lower and stable value. The primary cause of the dissipation is identified as the wavy or bending modes and contributions from radial modes has not been detected.

Excitation of wavy deformation was identified as detrimental to the operation of DWNT oscillators in previous studies, particularly with long shuttling inner nanotubes [13]. Observations reported in the present work are of qualitatively similar nature, wherein at first the sleeve sustains a translational motion by extracting a part of its rotational kinetic energy. The linear actuation decays subsequently via excitation of wavy deformations.

We have studied the (4, 4)/(9, 9) bearing system extensively. In addition, we have examined various other DWNT configurations chosen such that the inter-tube distance is as close to 0.34 nm as possible, which is similar to the equilibrium distance between adjacent sheets in graphite. For the similar system geometry (i.e. the short sleeve), a (6, 6)/(19, 0) bearing yielded angular velocity stabilization when ω_0 falls between 1.5 and 2.25 rad ps^{-1}. The rest of the configurations that we examined showed no such dissipative trend. This indicates that the observed characteristics of rotational bearings in this work may be specifically configuration-dependent. In the event of technological progress making the realization of DWNT- or MWNT-based devices possible, the need for precise geometries and specified chiralities can be envisaged to arise. We have shown that the operational characteristics of nanobearings can be considerably dependent upon their configuration. Through identifying different operational regimes and energy dissipation mechanisms, efforts can be driven towards improving the device performance. We thus hope that the current work can serve to assist in the efficient design and operation of such devices.

Some experimental studies have reported the use of MWNT systems with a set of

short outer tubes acting as mobile elements [32]. It was also observed that the actuation of axial motion of the sleeve is relatively easy and can be achieved via mechanical means as well as by imposing a small thermal gradient along the shaft. Their proposed usage as cargo movers may turn out as significant in the designs of futuristic nanomachines. The current work may find repercussions in the context of such device components with short-sleeved geometries.

4. Conclusions

In conclusion, we report a peculiar behaviour exhibited by a short-sleeved (4, 4)/(9, 9) DWNT rotational bearing. We find that, when initiated at certain specific initial angular velocities, the bearing is characterized by angular velocity plateaus when it attempts to sustain itself in a nearly wearless rotation. However, the tendency of smooth rotation can get interrupted by some energy dissipation mechanisms. Through a detailed analysis we demonstrate that the actuation of axial sliding of the sleeve serves as a channel to excite further dissipative wavy deformation modes in the inner tube. The excitation of wavy modes drives the bearing out of its smooth operating regime at a higher angular speed to a lower one. The observed phenomenon is qualitatively similar to the counterpart effects observed in the case of relative linear inter-tube motion in DWNTs. In low temperature operation, smooth rotational dynamics at certain angular velocity plateaus can persist for a few nanoseconds. The rotational stabilization is found to be subdued when the bearing operates at a high temperature due to enhanced frictional effects. These interesting aspects of the operation of short-sleeved nanobearings warrant further investigation and work along this line is in progress.

Encouraging technological developments suggest that in nanomachines based on DWNTs or MWNTs, their various configurations can serve as functional devices. Short-sleeved structures mounted on long shafts, for example, can be envisaged as cargo movers at the molecular scale. Considering the significance of precise operational control in such devices, in a general sense, the current work sheds light on new features of the configuration-dependent operation of nanobearings.

Acknowledgments

We thank Zhiping Xu for enlightening discussions and comments. Support from the Singapore Ministry of Education through the Academic Research Fund (Tier 2) under project no. T207B1214 is gratefully acknowledged.

References

[1] Saito D G Rand Dresselhaus M S 1998 *Physical Properties of Carbon Nanotubes* (London: Imperial College Press)
[2] Cumings J and Zettl A 2000 *Science* **289** 602
[3] Yu M F, Yakobson B I and Ruoff R S 2000 *J. Phys. Chem.* B **104** 8764
[4] Bourlon B, Glattli D C, Miko C, Forro L and Bachtold A 2004 *Nano Lett.* **4** 709
[5] Fennimore A M, Yuzvinsky T D, Han W Q, Fuhrer M S, Cumings J and Zettl A 2003 *Nature* **424** 408
[6] Yao N and Lordi V 1998 *Phys. Rev.* B **58** 12649
[7] Popescu A, Woods L M and Bondarev I V 2008 *Nanotechnology* **19** 435702
[8] Gong X J, Li J Y, Lu H J, Wan R Z, Li J C, Hu J and Fang H P 2007 *Nat. Nanotechnol.* **2** 709
[9] Joseph S and Aluru N R 2008 *Phys. Rev. Lett.* **101** 064502
[10] Kang J W and Hwang H J 2004 *Nanotechnology* **15** 1633
[11] Zheng Q S and Jiang Q 2002 *Phys. Rev. Lett.* **88** 045503
[12] Legoas S B, Coluci V R, Braga S F, Coura P Z, Dantas S O and Galvao D S 2003 *Phys. Rev. Lett.* **90** 055504
[13] Zhao Y, Ma C C, Chen G H and Jiang Q 2003 *Phys. Rev. Lett.* **91** 175504
[14] Servantie J and Gaspard P 2003 *Phys. Rev. Lett.* **91** 185503
[15] Servantie J and Gaspard P 2006 *Phys. Rev.* B **73** 125428
[16] Servantie J and Gaspard P 2006 *Phys. Rev. Lett.* **97** 186106
[17] Tangney P, Louie S G and Cohen M L 2004 *Phys. Rev. Lett.* **93** 065503
[18] Zhang S L, Liu W K and Ruoff R S 2004 *Nano Lett.* **4** 293
[19] Zhu C Z, Guo W L and Yu T X 2008 *Nanotechnology* **19** 465703
[20] Zhu B E, Pan Z Y, Wang Y X and Xiao Y 2008 *Nanotechnology* **19** 495708
[21] Guo W L, Zhong W Y, Dai Y T and Li S A 2005 *Phys. Rev.* B **72** 075409
[22] Wong L H, Zhao Y, Chen G H and Chwang A T 2006 *Appl. Phys. Lett.* **88** 183107
[23] Liu P, Gao H J and Zhang Y W 2008 *Appl. Phys. Lett.* **93** 083107
[24] Xu Z P, Zheng Q S, Jiang Q, Ma C C, Zhao Y, Chen G H, Gao H and Ren G X 2008 *Nanotechnology* **19** 255705
[25] Tangney P, Cohen M L and Louie S G 2006 *Phys. Rev. Lett.* **97** 195901
[26] Mayo S L, Olafson B D and Goddard W A 1990 *J. Phys. Chem.* **94** 8897
[27] Rivera J L, McCabe C and Cummings P T 2003 *Nano Lett.* **3** 1001
[28] Xu Z P, Zheng Q S and Chen G H 2007 *Phys. Rev.* B **75** 195445
[29] Tournier A L and Smith J C 2003 *Phys. Rev. Lett.* **91** 208106
[30] Karplus M and Kushick J N 1981 *Macromolecules* **14** 325
[31] Hess B, Kutzner C, van der Spoel D and Lindahl E 2008 *J. Chem. Theory Comput.* **4** 435
[32] Barreiro A, Rurali R, Hernandez E R, Moser J, Pichler T, Forro L and Bachtold A 2008 *Science* **320** 775

List of Figures

During 200–300 ps, the sleeve undergoes large axial displacement in a step-like fashion. (d) In 300–400 ps the translation of the sleeve is far ranged and step-like features are absent. After the dissipative period, during (e) 400–500 ps and (f) 500–600 ps, the step-like axial motion re-emerges.

Fig. 8 For a (4, 4)/(9, 9) DWNT configuration with 1.84 nm long sleeve containing a vacancy defect and 9.7 nm long inner tube, the potential energy profile as a function of displacement of the sleeve along the nanotube axis from its equilibrium position. The inset shows a magnified section of the same plot for the axial displacement of sleeve from 0 to 3 nm. The inset carries the same units on both the axes as the main plot.

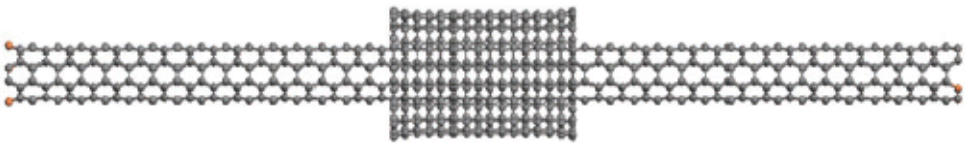

Fig. 1.

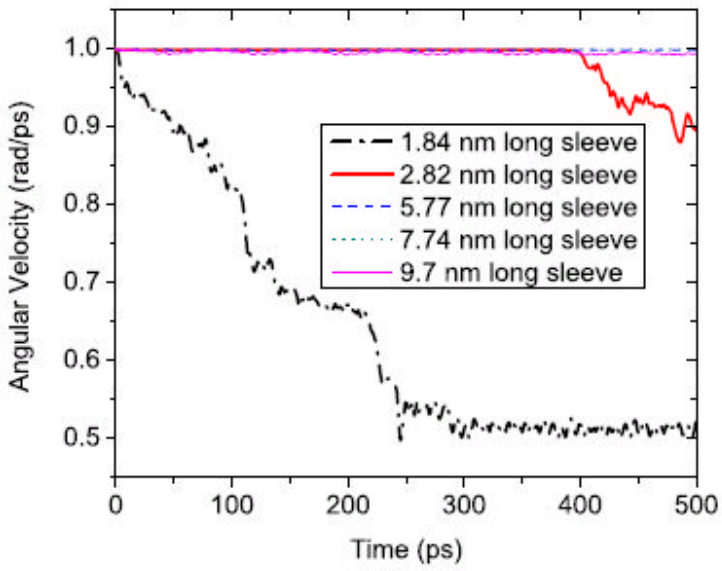
Angular Velocity (rad/ps)
1.0
0.9
0.8
0.7
0.6
0.5
0
100
200
300
400
500
Time (ps)
1.84 nm long sleeve
2.82 nm long sleeve
5.77 nm long sleeve
7.74 nm long sleeve
9.7 nm long sleeve

Fig. 2.

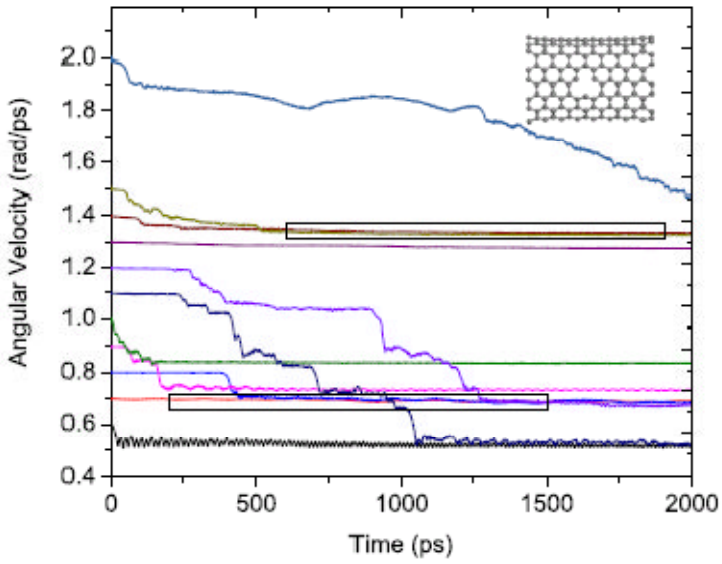
Angular Velocity (rad/ps)
2.0
1.8
1.6
1.4
1.2
1.0
0.8
0.6
0.4
0
500
1000
1500
2000
Time (ps)

Fig. 3.

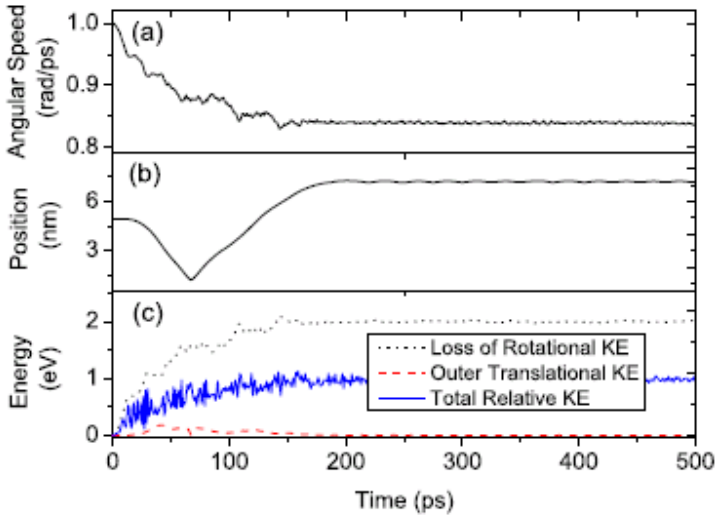
Angular Speed (rad/ps)
1.0
0.9
0.8
(a)
Position (nm)
6
3
(b)
Energy (eV)
2
1
0
(c)
Loss of Rotational KE
Outer Translational KE
Total Relative KE
0
100
200
300
400
500
Time (ps)

Fig. 4.

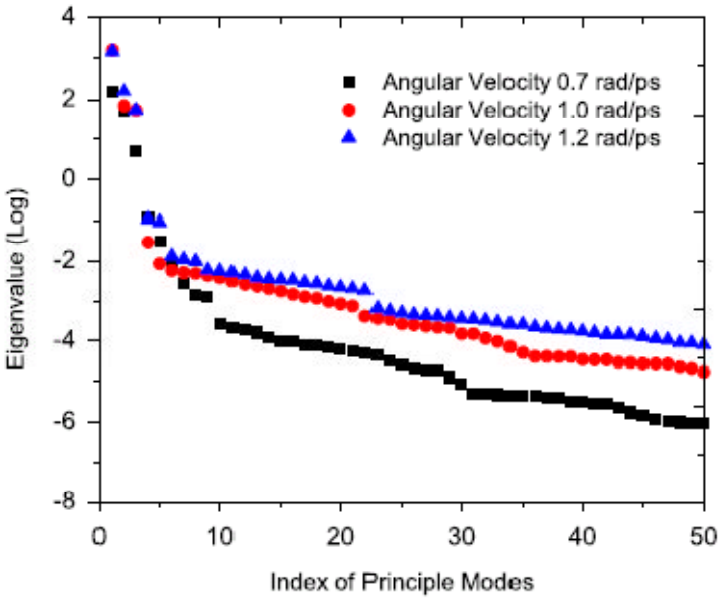
Angular Velocity 0.7 rad/ps
Angular Velocity 1.0 rad/ps
Angular Velocity 1.2 rad/ps
Eigenvalue (Log)
Index of Principle Modes
4
2
0
-2
-4
-6
-8
0
10
20
30
40
50

Fig. 5.

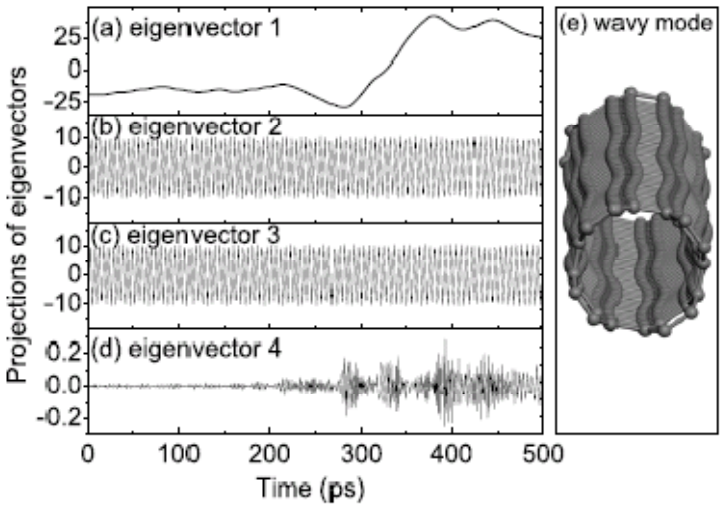
(a) eigenvector 1
(b) eigenvector 2
(c) eigenvector 3
(d) eigenvector 4
(e) wavy mode
Projections of eigenvectors
Time (ps)
25
0
-25
10
0
-10
10
0
-10
0.2
0.0
-0.2
0
100
200
300
400
500

Fig. 6.

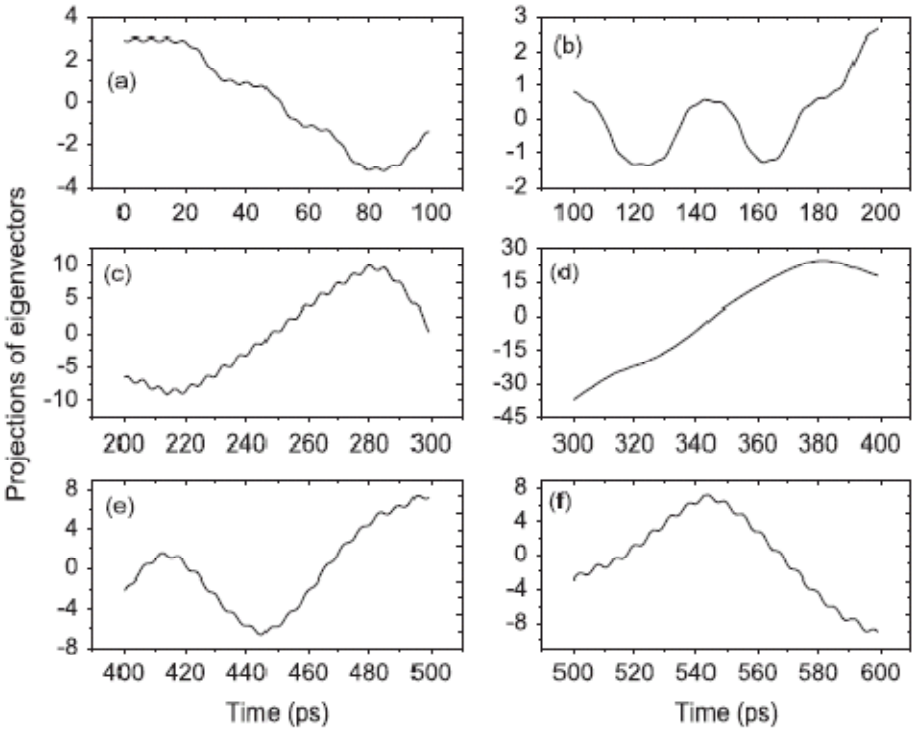

Fig. 7.

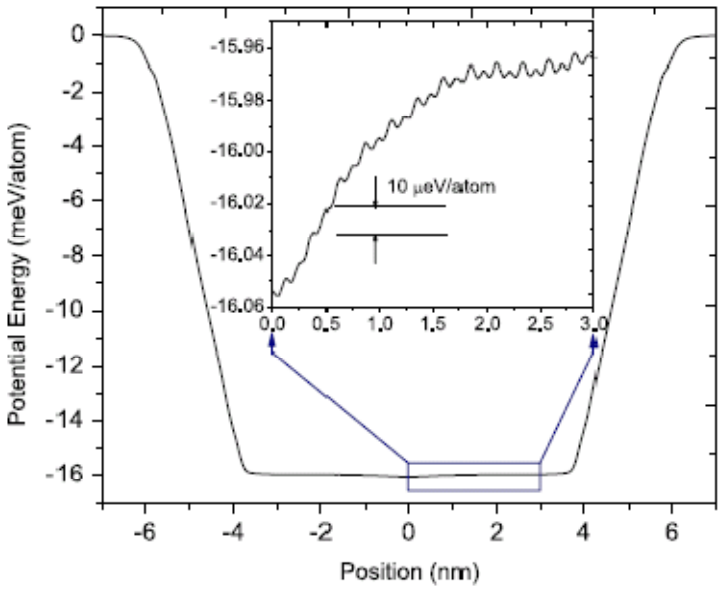

Fig. 8.